Applied and Environmental Microbiology, Jan. 2008, p. 437–445 Vol. 74, No. 2
0099-2240/08/$08.00+0 doi:10.1128/AEM.01688-07

Implications of Rewiring Bacterial Quorum Sensing▽†

Eric L. Haseltine and Frances H. Arnold*

Division of Chemistry and Chemical Engineering 210-41, California Institute of Technology, Pasadena, California 91125

Received 23 July 2007/Accepted 13 November 2007

Bacteria employ quorum sensing, a form of cell-cell communication, to sense changes in population density and regulate gene expression accordingly. This work investigated the rewiring of one quorum-sensing module, the *lux* circuit from the marine bacterium *Vibrio fischeri*. Steady-state experiments demonstrate that rewiring the network architecture of this module can yield graded, threshold, and bistable gene expression as predicted by a mathematical model. The experiments also show that the native *lux* operon is most consistent with a threshold, as opposed to a bistable, response. Each of the rewired networks yielded functional population sensors at biologically relevant conditions, suggesting that this operon is particularly robust. These findings (i) permit prediction of the behaviors of quorum-sensing operons in bacterial pathogens and (ii) facilitate forward engineering of synthetic gene circuits.

In bacteria, broadcasting of metabolite or small peptide signaling molecules enables sensing of changes in population density (18, 37, 57). This mechanism, known as quorum sensing, has been implicated in regulating the virulence factors in a number of bacterial pathogens, such as *Vibrio cholerae* (61), the bacterium responsible for the severe diarrheal disease cholera; *Pseudomonas aeruginosa* (30), the opportunistic pathogen responsible for death in cystic fibrosis patients and high mortality rates in immunocompromised individuals; and *Staphylococcus aureus* (32), a major culprit of infections in surgical wounds. Consequently, improved understanding of quorum-sensing regulation should provide more insight into combating these pathogens by using either traditional chemotherapy or emerging technologies such as quorum-sensing inhibitors (40) or regulated degradation of quorum-sensing signals (13, 14).

The *lux* module of the marine bacterium *Vibrio fischeri*, a facultative symbiont of luminescent fish or squid, serves as one model system for understanding quorum sensing. *V. fischeri* employs the *lux* module to regulate gene expression as a function of the population density. The key element of this system is a regulatory cassette consisting of the genes encoding LuxI and LuxR. LuxI is an acylhomoserine lactone (acyl-HSL) synthase; LuxR is a transcriptional regulator activated by the acyl-HSL. The acyl-HSL signaling molecule is produced inside the cell but can freely diffuse across the cell membrane into the environment. Therefore, the acyl-HSL concentration is low at low cell density. As the cell density increases, the signal accumulates in the environment and inside the cell. The signal can then bind LuxR to stabilize the transcription factor, which then activates gene expression. This process, in which activation of gene expression occurs only after attaining a critical cell density, is known as autoinduction.

In this work, we sought to computationally and experimentally address the fundamental question of how bacteria regulate cell-cell communication. Quorum sensing is often described in terms of a discrete switch; at low cell densities, the signal molecule is present at low concentrations, while at high cell densities, the signaling molecule accumulates to a concentration sufficient to activate gene expression (19). Meanwhile, the emergence of the synthetic gene circuit discipline has reemphasized the importance of accounting for the continuous nature of gene regulation (24). In this spirit, we sought to ascertain how quorum-sensing regulation works as a function of the population density in both a qualitative and a quantitative fashion. This goal differs from many of the recent characterizations of the *lux* system (15, 44, 51) because we examined the behavior of the entire regulatory module, not just a subset of it. Several synthetic-biology works have employed the entire *lux* regulatory module (3, 5, 6, 28, 59), but the focus of these works has been to achieve a desired engineering goal, not to characterize how the *lux* module functions.

One of the original published studies of quorum sensing in *V. fischeri* elegantly illustrated the autoinduction of bioluminescence as a function of cell density (43), and computational modeling hypothesized that this autoinduction resulted from bifurcation due to positive feedback on the *lux* regulatory elements (27). Yet, this characterization is far from complete. The simple *lux* module consists of three regulatory components, *luxR*, *luxI*, and the *lux* promoter; the native *lux* operon reflects merely one possible combination of these components. Combinatorial reshuffling of regulatory components has been shown to yield diverse logical outputs (23), and applying the same strategy to the *lux* system should elucidate possible responses of other quorum-sensing systems. Additionally, it is unclear how simple rearrangements in network architecture combined with system-specific parameters (e.g., transcriptional regulation and translational efficiency) will affect circuit performance. Specifically, do these rearrangements render functional circuits over biologically relevant conditions? If so, then the responses of these rearrangements can be used to predict the responses of other naturally occurring quorum-sensing operons. Finally, the computational prediction of bifurcation in the native *lux* operon has not been experimentally demonstrated. In this paper, we seek to address each of these issues.

* Corresponding author. Mailing address: Division of Chemistry and Chemical Engineering 210-41, California Institute of Technology, Pasadena, CA 91125. Phone: (626) 395-4162. Fax: (626) 568-8743. E-mail: frances@cheme.caltech.edu.

† Supplemental material for this article may be found at http://aem.asm.org/.

▽ Published ahead of print on 26 November 2007.

MATERIALS AND METHODS

Bacterial strains, media, and growth conditions. The bacterial strain used in this study was *Escherichia coli* DH5α [F^- φ80d*lacZ*Δ*M15* Δ(*lacZYA-argF*)*U169 deoR recA1 endA1 hsdR17*(r_K^- m_K^+) *phoA supE44* λ^- *thi-1 gyrA96 relA1*]. *E. coli* was cultured at 37°C in Luria-Bertani (LB) medium or on LB agar plates. The acyl-HSL used in this study was 3-oxohexanoyl-DL-homoserine lactone (3OC6HSL; Sigma Aldrich). Antibiotics were added at concentrations of 50 μg/ml kanamycin and 100 μg/ml chloramphenicol to maintain the plasmids.

Construction of the quorum-sensing plasmids used in this work. Plasmids pGLRKM-101, pPSSUB-101, and pPSSUB-102 were the kind gifts of Ron Weiss (Princeton University). Plasmids pPSSUB-101 and pLuxRI were described previously by Basu et al. (6) and You et al. (59), respectively. Both pPSSUB-101 and pPSSUB-102 contain a destabilized version of green fluorescent protein, GFPLVA [originating from pGFP(LVA); BD Biosciences Clontech], which in *E. coli* has a reported half-life of 40 min (2) and a rapid maturation time (detectable after only 10 min under fed-batch conditions [41]). pluxG-102 was constructed by using overlap extension PCR (25) to fuse the *luxR* promoter from pGLRKM-101 (3-G2-lux and 5-G-NotI) with *luxR* and its ribosome binding site (RBS) from pLuxRI (5-G2-lux and 3-XhoI-LuxR). The primers used to amplify the respective fragments are in parentheses; for the sequences of these primers, see Table S1 in the supplemental material. The resulting fragment was cloned into pPROLar.A122 (BD Biosciences Clontech) between the XhoI and NotI sites. pluxG-102C is identical to pluxG-102, except for the RBS. PCR was used to introduce a new *luxR* RBS (5-G-NotI and 3-KpnI-GC). The resulting fragment was cloned into pluxG-102 between the NotI and KpnI sites. pluxG-103 was constructed by amplifying the *luxI* gene from pLuxRI (5-Rseq and 5-AatII-LuxI). The resulting fragment was cloned into pluxG-102 between the AatII and BamHI sites. pluxRp-101 was constructed by using overlap extension PCR to fuse the *luxI* promoter from pPSSUB-101 (5-SalI-plux and 3-pluxC) with the *luxR* gene from pluxG-102 (5-LuxRC and 5-seq). The resulting fragment was cloned into pPROLar.A122 between the SalI and BamHI sites. pluxRp-103 is identical to pluxRp-101, except that a KpnI site was introduced upstream of the *luxR* gene. Overlap extension PCR was used to introduce this site (5-Rp-SalI and 3-Rp-3 and 5-Rp-3 and 3-HindIII-LuxRa). The resulting fragment was cloned into pluxRp-101 between the SalI and HindIII sites. pluxRp-103E is identical to pluxRp-103, except for the RBS. PCR was used to introduce a new *luxR* RBS (5-Rp-SalI and 3-KpnI-RpE). The resulting fragment was cloned into pluxRp-103 between the SalI and KpnI sites. All constructs were verified by DNA sequencing. For plasmid maps of these constructs, see Fig. S1 in the supplemental material.

Periodic-dilution experiments. Steady states of quorum-sensing constructs were assayed by using a periodic-dilution experiment to maintain the cultures in the growth phase; a similar experiment outlined by Chen and Weiss (9) served as the template for the following procedure. One-milliliter cultures in LB medium with the appropriate antibiotics were started from plates and grown for roughly 8 h at 37°C. A portion of the 1-ml culture was diluted into 50- or 100-ml cultures of LB medium containing 0.05 M morpholinepropanesulfonic acid (MOPS; pH 7.0) and the appropriate antibiotics (hereafter called LBM) and then grown at 37°C with shaking for 15 h to appropriate densities. When noted, these overnight cultures were induced with 3OC6HSL at 11 h into the growth step. The overnight cultures were transferred to 50-ml centrifuge tubes, pelleted, washed, repelleted, and then resuspended to the desired absorbance (A_{600}; all absorbance readings in this report were performed at 600 nm) in LBM. The resuspensions were diluted with LBM in 48-well blocks to various absorbances at a final volume of 2.2 ml. The absorbance and fluorescence (excitation at 470 nm, emission at 509 nm, gain of 69) of a 200-μl volume were assayed in a 96-well microplate with a clear bottom (Corning Costar) by using a microtiter plate reader (Infinite M200; Tecan); this reading corresponds to the $t = 0$ h measurement. The blocks were then covered with Aeroseal (Daigger) and shaken at 37°C. At the end of each hour, the absorbance and fluorescence of 200 μl were assayed; note that the $t = 0$ h measurement corresponds to the reading at the beginning of the hour as opposed to the end. A portion of each culture was then removed, and fresh LBM was added to reset the initial absorbance to a predetermined constant value while maintaining the culture volume at 2 ml. For the absorbance-CFU/ml calibration curve used to calculated the volume removed, see Fig. S2 in the supplemental material. This curve fits the data using the Hill function

$$A_{600} = \frac{c_1 r^{c_3}}{1 + r^{c_3}} + c_4 \tag{1}$$

$$r = \frac{\text{CFU/ml}}{c_2} \tag{2}$$

in which $c_1 = 2.93$, $c_2 = 3.77 \times 10^8$ CFU/ml, $c_3 = 1.02$, and $c_4 = 0.0445$. This process was repeated seven or eight times until both the absorbance and fluorescence values equilibrated. At this time, the cultures were pelleted, decanted, washed in 1 ml phosphate-buffered saline (PBS; pH 7.0), pelleted, decanted, and resuspended in 1.8 ml PBS. The absorbance and fluorescence of 200 μl were again assayed. Absorbance and fluorescence readings were corrected by subtracting the respective readings of 200 μl PBS. If the corrected fluorescence readings were nonpositive, then the cultures were resuspended to an A_{600} of ~0.3 and assayed again. All steady-state measurements correspond to the corrected absorbance reading in LBM medium and the fluorescence or absorbance reading in PBS at the final time point. Unless otherwise noted, the results from at least three different experiments (each experiment being started from a different colony) were used to calculate the means (points) and standard deviations (error bars) shown in each of the steady-state figures. Also, samples were drawn at the next to last time point to (i) measure the number of viable cells by serial dilution and plating and (ii) confirm the accuracy of the calibration curve.

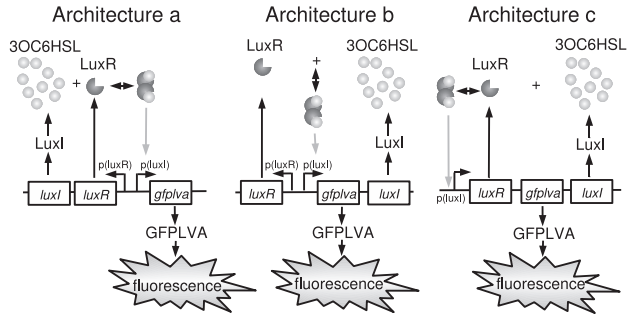

FIG. 1. Possible architectures for quorum-sensing gene circuits. Architecture a: constitutive expression of *luxI* and *luxR*, *p*(*luxI*)-regulated expression of *gfplva*. Architecture b: constitutive expression of *luxR*, *p*(*luxI*)-regulated expression of *luxI* and *gfplva*. Architecture c: *p*(*luxI*)-regulated expression of *luxI*, *luxR*, and *gfplva*.

Modeling of the *lux* system. Urbanowski et al. (53) determined the binding characteristics of the LuxR protein to the *lux* promoter. Gel shift experiments and DNA protection assays demonstrated that stimulation of LuxR-DNA complex formation by varying either the 3OC6HSL or the LuxR concentration is noncooperative (Hill coefficients of 0.9 and 0.85, respectively). One kinetic mechanism that captures both of these features is the following model:

$$2A + 2R \overset{K_1}{\rightleftharpoons} R^* \quad K_1 = \frac{c_{R^*}}{c_A c_R} \tag{3}$$

$$R^* + P_0 \overset{K_2}{\rightleftharpoons} P_1 \quad K_2 = \frac{c_{P_1}}{c_{R^*} c_{P_0}} \tag{4}$$

in which A is the 3OC6HSL signaling molecule, R is the LuxR protein, R^* is the activated transcription factor, P_0 is the unbound DNA, P_1 is the LuxR-DNA complex, and c_j refers to the concentration of species j. For this model,

$$K_1 K_2 = \frac{c_{P_1}}{c_{P_0} c_A c_R} \text{ and } \log(K_1 K_2) + \log c_A + \log c_R = \log\left(\frac{c_{P_1}}{c_{P_0}}\right) \tag{5}$$

Plotting the right-hand side of equation 5 as a function of the logarithm of either A or R renders the Hill plot. It is clear that such a plot would give a Hill coefficient of 1.0 for varying the concentration of either A or R while holding the other concentration constant. Hence, this mechanism captures the essential features of the gel shift experiments and DNA protection assays.

Models were analyzed by using the continuation package CL_MATCONT, a variant of the MATCONT package (11), to solve for the steady states as a function of the population density. The modeling results presented in this paper assume that the system is in a continuous-flow setting; see section S1 in the supplemental material for a more detailed account of this modeling. Modeling the system discretely to describe the periodic-dilution experiment did not significantly alter the qualitative or quantitative results because the growth time of 1 h between dilutions was relatively short (data not shown).

TABLE 1. Plasmids used in this study[a]

Architecture	Product(s)	Plasmid(s)
a	LuxR + LuxI	pluxG-103
	GFPLVA	pPSSUB-101
b	LuxR	pluxG-102, pluxG-102C
	GFPLVA + LuxI	pPSSUB-102
c	LuxR	pluxRp-101, pluxRp-103E
	GFPLVA + LuxI	pPSSUB-102

[a] Constructs in the same row differ only in the promoter region (−20 to −1 positions upstream of the first gene), which effectively alters the RBS.

RESULTS

The mathematical model predicts that shuffling of the network architecture can result in graded, threshold, or bistable gene expression. Given the reporter gene *gfplva* and the *luxI* and *luxR* components, there are three possible ways of regulating GFPLVA expression as a function of population density. These shuffled network architectures are illustrated in Fig. 1. Here, *p*(*luxI*) and *p*(*luxR*) refer to the *luxI* and *luxR* promoters in the native *lux* operon. In architecture a, *luxI* and *luxR* are constitutively expressed from the *p*(*luxR*) promoter and *gfplva* is expressed from the *p*(*luxI*) promoter. In architecture b, *luxR* is constitutively expressed from the *p*(*luxR*) promoter and *luxI* and *gfplva* are expressed from the *p*(*luxI*) promoter. Modeling suggests that exchanging the placement of *luxI* and *luxR* in this architecture yields behavior similar to that which results from nominal architecture b since LuxI and LuxR demonstrate comparable cooperativities, although the precise behavior of the circuit depends on the parameter values. Finally, in architecture c, *luxI*, *luxR*, and *gfplva* are all expressed from the *p*(*luxI*) promoter. The network architectures presented in Fig. 1 correspond experimentally to the plasmid combinations outlined in Table 1.

To explore the possible ranges of system behavior, we constructed mass action kinetic models for all three of the architectures in Fig. 1; Fig. 2 presents these models. All reactions are elementary as written except for cell growth, which is assumed to follow a logistic growth expression, and the transcription factor binding events, whose expressions are given by equations 3 and 4. These models represent a highly simplified version of the actual system; transcription and translation are lumped into first-order processes limited by a DNA catalyst, a simple expression approximates cell growth, and the transcription factor binding reactions are assumed to be at equilibrium. We also assume that the signaling molecule freely diffuses into and out of the cell membrane, whereas all of the other intracellular species cannot freely diffuse. Finally, we assume that the system is well mixed and deterministic.

Figure 3 plots the steady-state response of each network architecture for GFPLVA fluorescence per cell as a function of cell density. Network architecture a leads to a graded response; fluorescence per cell increases linearly with cell density on a log-log scale until the fluorescence saturates. In contrast, network architecture b results in a threshold response characteristic of a soft switch; below (above) a certain density, the fluorescence per cell is minimal (maximal). This threshold-like behavior stems directly from the positive feedback on the signaling molecule obtained by placing the *luxI* gene under the control of the *p*(*luxI*) promoter. Finally, network architecture c exhibits bistability over a range of densities. Note that the middle loci of steady states are unstable. Here, fluorescence per cell is hysteretic in that either maximal or minimal fluorescence results, depending upon the initial condition of the system.

In continuous-growth cultures, the presence of bistability can be detected by varying the initial concentration of the signaling molecule, 3OC6HSL. Because bistability results in two stable steady states (or attractors) for a given density, the initial 3OC6HSL concentration can determine to which steady state the system evolves. Figure 3d presents a phase portrait in two dimensions (3OC6HSL concentration and population density) for a simplified model of the system. Here, starting the experiment from the same population density but different initial concentrations of 3OC6HSL leads to different steady-state attractors.

Previous work indicates that LuxR is capable of positively

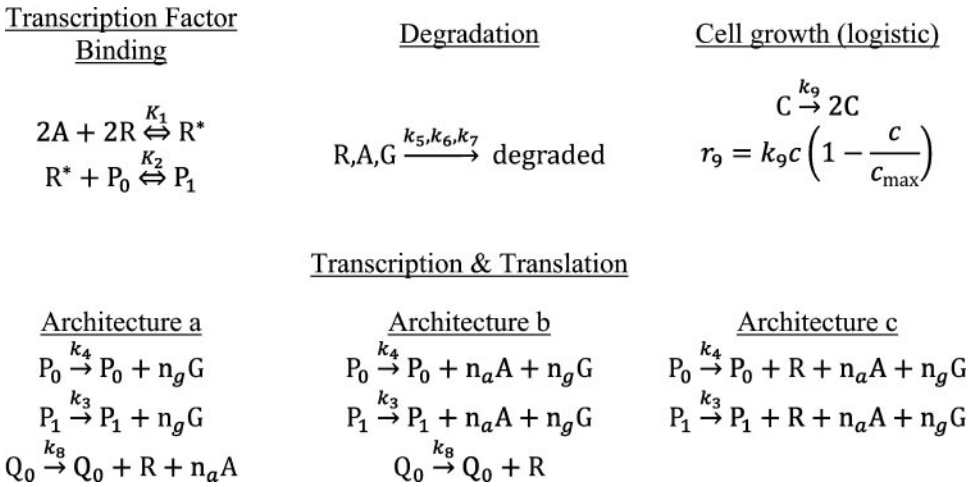

FIG. 2. Kinetic mechanisms used to model the behaviors of the three design architectures. G, C, and Q_0 refer to GFPLVA, bacterial cells, and the DNA encoding constitutive expression, respectively.

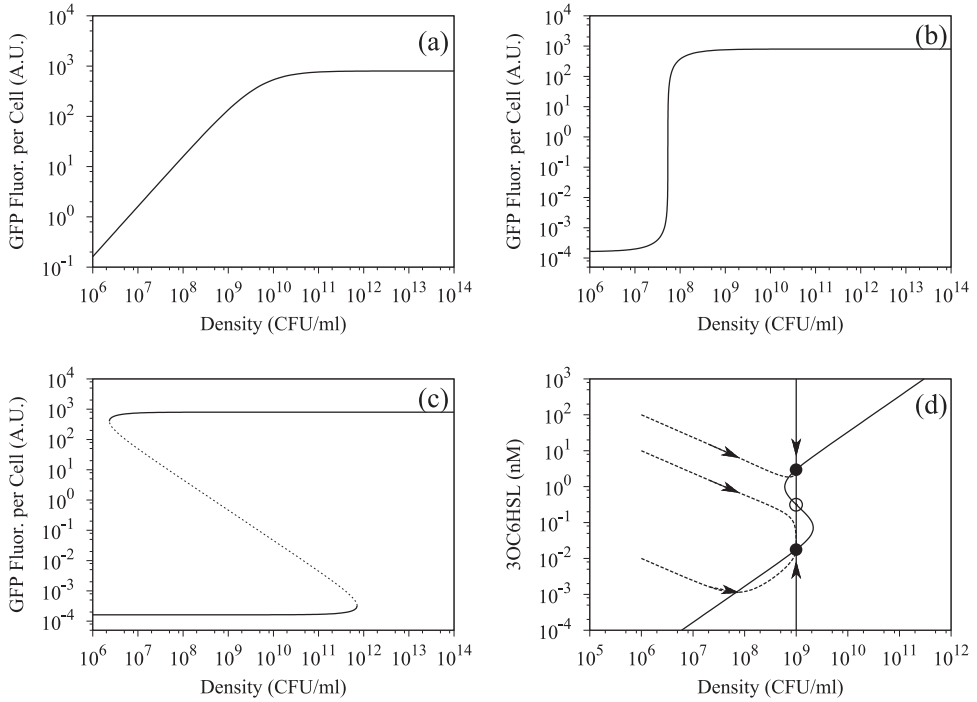

FIG. 3. Qualitative steady-state behaviors of (a) design architecture a, constitutive expression of both *luxR* and *luxI*; (b) architecture b, constitutive expression of *luxR* and *p*(*luxI*)-mediated expression of *luxI*; and (c) architecture c, *p*(*luxI*)-mediated expression of both *luxI* and *luxR* (the dashed line denotes the unstable loci of steady states). Plot d presents a phase plot for a simplified model of the system illustrating the dependence of the steady state on the initial condition (both cell density and 3OC6HSL concentration) for a steady-state cell density of 10^9 CFU/ml. Solid lines denote the null clines (where the derivative of either the cell density or the 3OC6HSL concentration is zero). Dashed lines denote representative phase traces for this system that were obtained by solving for time courses of the dynamic model with various initial conditions and projecting the solutions onto the cell density-3OC6HSL axes. Arrows denote the directionality of these traces, filled points denote stable attractors, and the unfilled point denotes the unstable attractor. Fluor., fluorescence; A.U., arbitrary units.

stimulating transcription from the *p*(*luxR*) promoter to a small degree (46, 48). In contrast, we have assumed that the *p*(*luxR*) promoter is constitutive. This discrepancy does not significantly affect the model predictions because the observed positive feedback from the *p*(*luxR*) promoter is significantly smaller than that observed from the *p*(*luxI*) promoter (48; also see section S2 in the supplemental material).

Shuffling the architecture of the *lux* operon yields graded, threshold, and bistable responses as predicted by the mathematical model. We constructed each of the three different network architectures shown in Fig. 1. Constitutive expression and *lux*-mediated expression were obtained by expressing genes from the *p*(*luxR*) and *p*(*luxI*) promoters, respectively. We then performed periodic-dilution experiments to

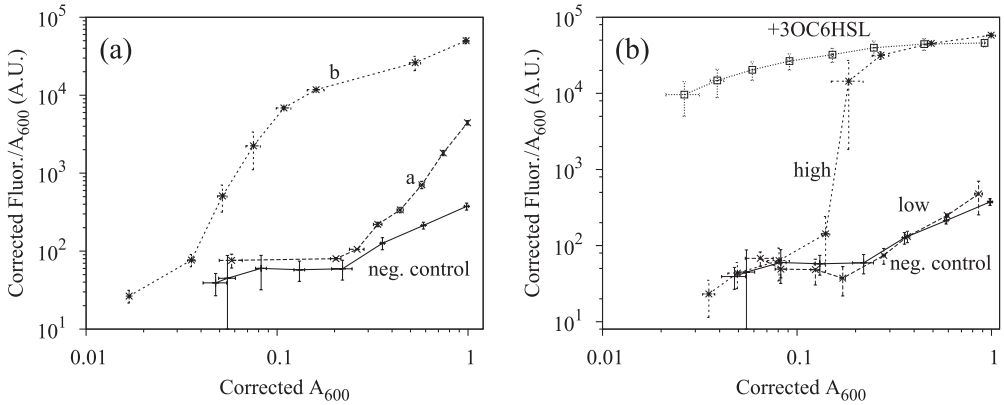

FIG. 4. Experimental steady-state results for architectures a, b, and c. In the bistable region, architecture c exhibits memory in that the initial condition can drive the system to different steady-state attractors, as demonstrated in plot b. Here, initial cultures were grown to a low absorbance (A_{600} of <0.2), grown to a high absorbance (A_{600} of >0.7), or induced with 100 nM 3OC6HSL. The negative (neg.) control results (pPROLar.A122 and pPSSUB-102) are plotted for comparison. Fluor., fluorescence; A.U., arbitrary units.

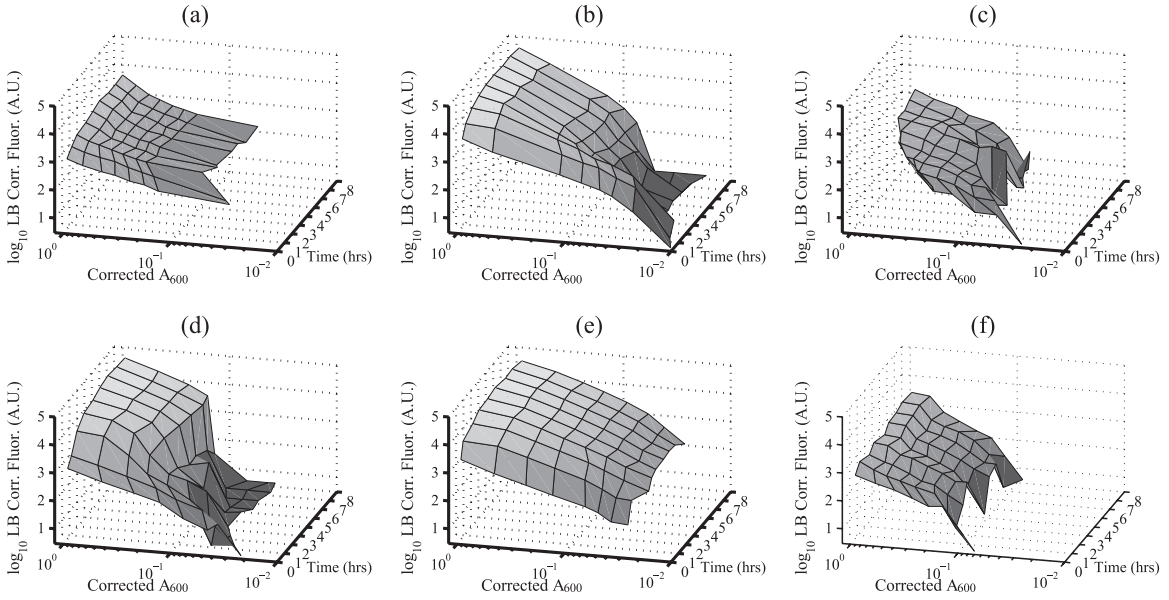

FIG. 5. Dynamic periodic-dilution results for the shuffled network architectures. Corrected absorbance and fluorescence dynamics over the duration of the periodic-dilution experiment are shown for (a) architecture a, (b) architecture b, (c) architecture c low (A^{o}_{600} of <0.2), (d) architecture c high ($A^{o}_{600} = 0.799$), (e) architecture c induced with 100 nM 3OC6HSL, and (f) the negative control. Architecture a is pluxG-103 and pPSSUB-101, architecture b is pluxG-102 and pPSSUB-102, architecture c is pluxRp-103E and pPSSUB-102, and the negative control is pPROLar.A122 and pPSSUB-102. A^{o}_{600} is the absorbance of the overnight culture used to start the periodic-dilution experiment. Each plot uses the same shading to highlight differences in the measured fluorescence values. Corr., corrected; Fluor., fluorescence; A.U., arbitrary units.

determine the steady-state behavior of each architecture. The results are presented in Fig. 4. The qualitative features of the shuffled architectures are consistent with the model predictions. Namely, shuffling the network architecture of the *lux* operon yields graded, threshold, and bistable responses, as predicted by the mathematical model and shown in Fig. 4.

The dynamic evolution of all of the architectures and the negative control is presented in Fig. 5 to illustrate both the dynamics of the periodic-dilution experiment and the notion of bistability. This figure demonstrates equilibration first of the absorbances in approximately 2 to 3 h and then the fluorescences in the last 5 to 8 h. Note that the *z* axis is a plot of the corrected fluorescence values (i) in LBM as opposed to PBS and (ii) not normalized by the absorbance reading. Also, the two highest absorbances in Fig. 5c did not equilibrate until later in the experiment since the experiment was started from a low-absorbance culture.

In the bistable region, the system exhibits memory in that the initial condition can drive the system to different steady-state attractors. Figure 5c to e illustrates the dynamics of this process for architecture c. Initiating the periodic-dilution experiment from a culture grown to a low initial absorbance (A^{o}_{600} of <0.2) maintains the system in a low-fluorescence state, whereas initiating the experiment from a culture induced with 100 nM 3OC6HSL results in high fluorescences for all of the densities tested. Initiating the experiment from a culture grown to a high initial absorbance (A^{o}_{600} of >0.7) results in density-dependent fluorescence. We also note that in each experiment, the same 1-ml inoculating culture was used to start a low culture and either a high or a 3OC6HSL culture. Thus, low fluorescence readings most likely resulted from the network architecture, as opposed to disabling of the quorum-sensing operon by, for example, mutation.

Shuffling the architecture of the *lux* operon yields functional population sensors. We sought to determine if shuffling of network architecture would give rise to functional quorum-sensing behavior in the observable range of the periodic-dilution experiment. We define a functional population sensor as "on" at high absorbances (A_{600} of ~ 1) and "off" at low absorbances (A_{600} of $<10^{-2}$). In the previous section, we tuned the circuit behavior to fall within the observable range by manipulating the *luxR* RBS. Here, we maintained as much similarity in terms of promoter regions and RBSs as possible. According to our definition of a functional population sensor, Fig. 6a demonstrates that shuffling the network architecture yields functional sensors for architectures a and b. Architecture c, however, results in maximal GFPLVA expression, regardless of the initial condition. Prolonged maintenance of this high-expression state appears to be unfavorable; this particular combination (pluxRp-101 and pPSSUB-102) did not equilibrate in the time course of the experiment (see Fig. S3 and section S3 in the supplemental material). pluxRp-101 and pluxRp-103E differ by only the *luxR* RBS strength (pluxRp-101 being stronger than pluxRp-103E), and Fig. 4b demonstrates that the combination of pluxRp-103E and pPSSUB-102 exhibits bistability. Thus, we infer that the bistable region of pluxRp-101 and pPSSUB-102 occurs at densities lower than those observable from the periodic-dilution experiment.

Given the same set of parameter values for each reaction event, the model should predict the observed steady-state results by only shuffling the network architecture. By adjusting parameters that had no experimental basis for their values, we identified a set of parameters consistent with the observed data

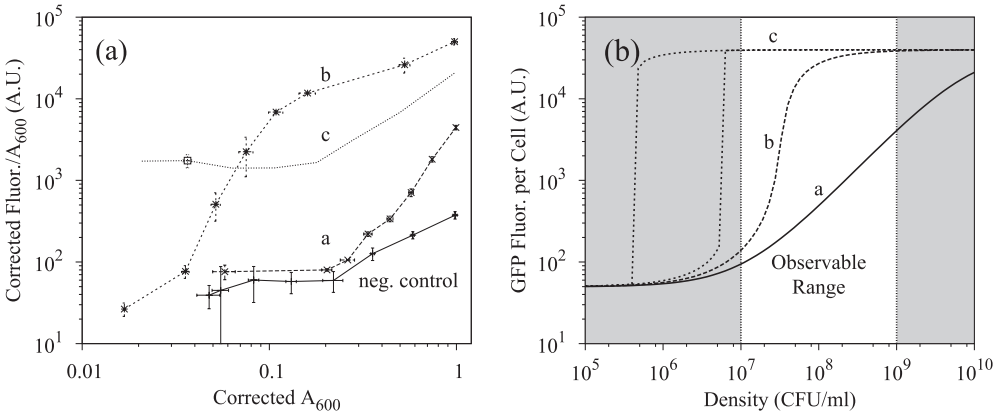

FIG. 6. Comparison of the *lux* operon with shuffled network architectures. Panels: a, experimental results; b, model predictions. Architectures a and b yield a functional response in the observable range of the periodic-dilution experiment. Note, however, that network architecture c does not exhibit bistability within this range. The unshaded region in plot b corresponds to the observable range of the periodic-dilution experiment (A_{600} of 0.01 to 1). The negative (neg.) control results (pPROLar.A122 and pPSSUB-102) are presented in plot a for comparison. Fluor., fluorescence; A.U., arbitrary units.

(see Table S3 in the supplemental material). The periodic-dilution experiment captures corrected absorbances within an A_{600} range of 0.01 to 1.0, corresponding to a range of roughly 10^7 to 10^9 CFU/ml. As shown in Fig. 6b, the model suggests that (i) the bistable region for architecture c occurs before the lowest density observable from the experiment and (ii) maximal induction of architecture a is achieved at densities higher than those observable from the experiment. Both predictions are consistent with the observed behavior.

The wild-type *lux* operon behavior is consistent with a threshold response. In the bistable region (if there is one), different initial conditions can drive the system to different steady-state attractors. To test the native *lux* architecture, namely, network architecture b, for bistability, we varied the initial condition in three ways. Three cultures were respectively grown to an initial absorbance below the induction threshold, an initial absorbance above the induction threshold, and an initial absorbance above the induction threshold induced with 10 μM 3OC6HSL. Here we define the induction threshold as the absorbance at which *p*(*luxI*)-mediated gene expression is activated. The nominal *luxR* configuration for architecture b (plasmid pluxG-102) induces the threshold response at a low initial absorbance (A_{600} of ~0.05; Fig. 6a). This low induction threshold made varying the initial condition difficult. Therefore, we altered the *luxR* RBS to increase the induction threshold (plasmid pluxG-102C), a manipulation suggested by the mathematical model as shown in Fig. 7a. Figure 7b presents the steady-state data confirming this model prediction.

Overnight cultures with different initial conditions were then used to start three respective periodic-dilution experiments using plasmids pluxG-102C and pPSSUB-102. For the evolution of the absorbances and fluorescences over time, see Fig. S4 in the supplemental material. After the system equilibrated (at $t = 8$ h), the system steady states were compared. Figure 8 demonstrates that, to the accuracy of the experiment, the steady states are virtually indistinguishable. Due to day-to-day variability in this experiment, the steady-state results for pluxG-102C and pPSSUB-102 presented in Fig. 8 were obtained from a single experiment. Comparing results from different days also demonstrates little difference in the steady states obtained from different initial conditions (see Fig. S5 in the supplemental material). These data do not completely rule out the possibility of bistability; for example, small positive feedback from the *luxR* promoter can lead to a small bistable region (see Fig. S7 in the supplemental material). Our data suggest that a bistable region, if present, is sufficiently small to render the behavior of the native *lux* architecture equivalent to a threshold-type response. Also, comparing Fig. 8 to Fig. 4b emphasizes that architecture c has a much larger region of bistability than architecture b.

DISCUSSION

The modeling and experimental results presented in this paper illustrate how simple changes in network architecture can dramatically alter the steady-state behavior of a cell-cell signaling network. Increasing the number of *lux* regulatory elements under the control of the *p*(*luxI*) promoter respectively yields graded, threshold, and bistable responses. Previous implementations of synthetic bistable gene circuits (4, 7, 21, 26, 29) have all required some degree of cooperativity. Here, the modeling suggests that bistability can be engineered from non-cooperative components by taking advantage of the fact that two components (3OC6HSL and LuxR) combine to form the activated transcription factor. Placing both *luxR* and *luxI* under the control of the *p*(*luxI*) promoter introduces a nonlinearity sufficient for bistability, as was demonstrated experimentally.

A previous modeling work suggested that the wild-type *lux* operon yields bistable behavior (27). The presence of bistability, however, has not been determined experimentally to the best of our knowledge. By manipulating the initial condition around the quorum-sensing induction density, we demonstrated that the response of the wild-type *lux* operon is more consistent with a threshold, as opposed to a bistable, response. We expect that understanding how different network architectures render different responses for the quorum-sensing system should provide valuable insight into designing new synthetic gene circuits. For example, several recent papers assume that

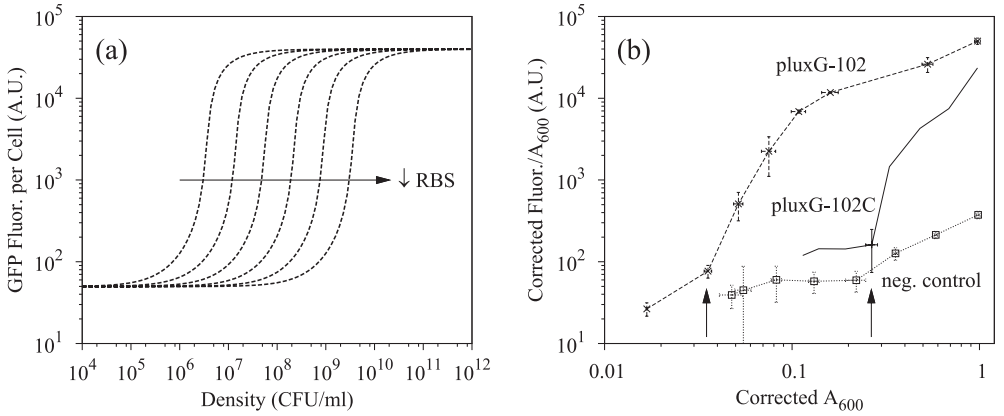

FIG. 7. Model prediction and experimental verification of the effect of altering *luxR* RBS strength. As shown in plot a, the model predicts that decreasing the *luxR* RBS strength increases the density of the induction threshold, that is, the minimum population density required for activation of the threshold response. Plot b verifies this prediction by comparing the responses for architecture b using plasmids pluxG-102 and pluxG-102C, which differ only by the *luxR* RBS. The arrows in plot b designate the induction threshold. The negative control results (pPROLar.A122 and pPSSUB-102) are presented in plot b for comparison. Fluor., fluorescence; A.U., arbitrary units.

formation of the activated *lux* transcription factor is either cooperative (49) or the result of elementary dimerization of two transcription factor-signaling molecule complexes (5, 36, 60). Coupled with positive feedback, both of these assumptions would lead to the erroneous prediction that architecture b (positive feedback on *luxI*) yields a significant bistable range. Using such assumptions in other modeling efforts will similarly yield incorrect predictions about the steady-state behavior of these engineered constructs.

The experimental results also raise questions about how the natural *lux* system evolved. Gene duplication, gene shuffling, and point mutations can each give rise to new genes and function (1). Recent theoretical and experimental results suggest that certain motifs are particularly "evolvable," in that new functions readily arise from either gene shuffling of regulatory and output elements (23), point mutations to operons with dynamical plasticity (34, 54), a combination of the two (17, 55), or gene duplication and divergence (50). The work presented in this paper suggests that simple rearrangements of the *lux* regulatory module can result in qualitatively different steady-state population level responses. Additionally, simple shuffling of the architecture can give rise to population sensors that induce at closely clustered population densities (within 10^6 to 10^8 CFU/ml). Thus, shuffling from one architecture to another could maintain a quantitatively functional population sensor. Such robustness may explain the spate of recent synthetic-biology works that have successfully reengineered this operon to obtain effective quorum-sensing behavior by using a variety of different architectures (3, 5, 6, 28, 44, 59). Also, if quorum sensing indeed descended from a common ancestral operon, then these results suggest that any of these behaviors might be found in current quorum-sensing architectures.

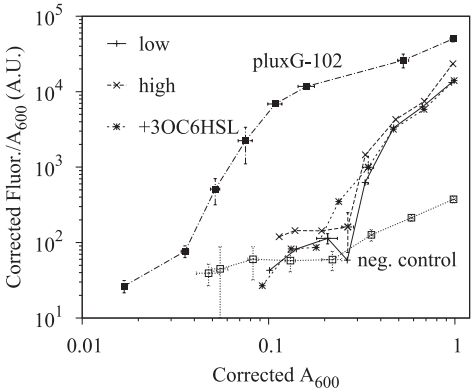

FIG. 8. Architecture b does not exhibit bistability under these circumstances. Here, initial cultures were grown to a low absorbance (A^{o}_{600} of <0.2), grown to a high absorbance (A^{o}_{600} of >0.7), or induced with 10 μM 3OC6HSL. For architecture b, consisting of pluxG-102C and pPSSUB-102, the same steady state is obtained, regardless of the initial conditions tested, to the accuracy of the experiment. The negative (neg.) control results (pPROLar.A122 and pPSSUB-102) are plotted for comparison. Fluor., fluorescence; A.U., arbitrary units.

Such a finding has particular import due to the fact that quorum sensing has been implicated as a global regulator of virulence in several human and agricultural pathogens (30, 31, 47, 61). The possibility of bistability arising in such pathogens could yield insight into understanding and controlling these pathogens. For example, recent modeling papers have predicted bistability in the regulation of the plant pathogen *Agrobacterium tumefaciens* (22) and the human pathogen *P. aeruginosa* (12, 16). If bistability is indeed present, then once virulence genes are turned on, the pathogen density must be reduced substantially below the induction density to turn off expression of the virulence factors. Elimination of the virulence factors themselves depends on the stability of these factors in the cellular milieu. Consequently, the virulence factors may not be readily down-regulated. Once quorum sensing is down-regulated, though, the bifurcation works in one's favor by making reinduction difficult. Unfortunately, the presence of bistability cannot be readily inferred by simply inspecting the DNA sequences of the quorum-sensing operons in pathogens. However, combining our findings with both existing knowledge of the operon structure and biochemical data on transcription factor cooperativity permits us to speculate as to the response of the quorum-sensing network. Namely, the modeling suggests that (i) a threshold response results from positive feed-

TABLE 2. Predicted behavior of the quorum-sensing circuits of gram-negative plant and human pathogens[a]

Pathogen	LuxI/LuxR homolog	Cooperative DNA binding	Feedback[b]	Predicted response	Reference(s)
Agrobacterium tumefaciens	TraR/TraI	No	+, TraR/TraI	Bistable	20, 62
Burkholderia cepacia	CepR/CepI	Yes	+, CepI	Bistable	58
Erwinia chrysanthemi	ExpR/ExpI	No	+, ExpI	Threshold	8, 42
Pantoea stewartii	EsaR/EsaI	No	−, EsaR	Threshold	38
Pseudomonas aeruginosa	LasR/LasI	No	+, LasI	Threshold	45

[a] Based on the experimentally observed cooperativity of DNA binding and the feedback on quorum-sensing elements.
[b] Plus and minus signs denote positive and negative feedback, respectively.

back on a single, noncooperatively bound regulatory element (either a LuxR or a LuxI homolog) and (ii) bistability results from either positive feedback on two noncooperatively bound regulatory elements or positive feedback on one or more cooperatively bound regulatory elements. Using these criteria, we predict, as shown in Table 2, that the LasR/LasI, EsaR/EsaI, and ExpR/ExpI systems should exhibit threshold responses while the TraR/TraI and CepR/CepI systems are capable of bistability. Bistability is likely a feature of gram-positive quorum-sensing pathogens as well. For example, *S. aureus* exhibits positive feedback on both the quorum-sensing signal and receptor (39). We stress that the presence of bistability should be rigorously examined in these systems by using either periodic-dilution experiments, as presented in this work, or by using other constant growth rate environments such as a chemostat or a turbidostat.

The difference in response for the LasR/LasI and CepR/CepI systems is particularly intriguing because (i) both systems are activated by the same acyl-HSL signal (3OC12HSL) and (ii) their respective hosts, *P. aeruginosa* and *B. cepacia*, are known to coinfect the lungs of cystic fibrosis patients, leading to impairment of lung function and eventually death (10). Interestingly, it appears that *P. aeruginosa* can induce the expression of quorum sensing-controlled virulence factors in *B. cepacia* under conditions in which *B. cepacia* cannot induce itself (35). These results suggest that (i) the population density of *B. cepacia* falls within its bistable region and (ii) the LasR/LasI system is inducing the CepR/CepI system. The coupling of these two species through a common signal renders a quorum-sensing response significantly different than the individual responses.

Understanding how cell-cell communication evolved in bacteria may provide insights into how such feedback evolved in higher organisms since combining such communication with positive feedback is a strategy employed by a wide variety of multi- and unicellular organisms to coordinate and regulate cellular decisions. In *Drosophila*, temporal gradients of regulatory proteins drive differential patterning of the embryo by using, for example, bistability generated by positive feedback on a signaling receptor (52, 56). In mammalian cells, interferon molecules secreted by virus-infected cells lead uninfected cells to up-regulate antiviral defenses via interferon-stimulated positive feedback (33). How might these complicated mechanisms have evolved? Our results suggest that the architecture of these systems might make them particularly evolvable. Namely, simple shuffling of finely tuned network architectures may render detuned yet functional operons with various degrees of positive feedback.

ACKNOWLEDGMENTS

E.L.H. gratefully acknowledges support from the Caltech Center for Biological Circuit Design and the National Institutes of Health under Ruth L. Kirschstein National Research Service Award 5F32CA120055. F.H.A. acknowledges support from the U.S. NSF and NIH.

We thank Ron Weiss, Subhayu Basu, and Ming-Tang Chen for providing genetic constructs and experimental advice. We also thank Cynthia Collins, Katie Brenner, Cara Tracewell, and Michael Dougherty for helpful discussions and experimental advice.

REFERENCES

1. **Alberts, B., A. Johnson, J. Lewis, M. Raff, K. Roberts, and P. Walter.** 2002. Molecular biology of the cell, 4th ed. Garland Science, New York, NY.
2. **Andersen, J. B., C. Sternberg, L. K. Poulsen, S. P. Bjørn, M. Givskov, and S. Molin.** 1998. New unstable variants of green fluorescent protein for studies of transient gene expression in bacteria. Appl. Environ. Microbiol. **64:**2240–2246.
3. **Anderson, J. C., E. J. Clarke, A. P. Arkin, and C. A. Voigt.** 2006. Environmentally controlled invasion of cancer cells by engineered bacteria. J. Mol. Biol. **355:**619–627.
4. **Atkinson, M., M. A. Savageau, J. T. Myers, and A. J. Ninfa.** 2003. Development of genetic circuitry exhibiting toggle switch or oscillatory behavior in *Escherichia coli*. Cell **113:**597–607.
5. **Basu, S., Y. Gerchman, C. H. Collins, F. H. Arnold, and R. Weiss.** 2005. A synthetic multicellular system for programmed pattern formation. Nature **434:**1130–1134.
6. **Basu, S., R. Mehreja, S. Thiberge, M.-T. Chen, and R. Weiss.** 2004. Spatiotemporal control of gene expression with pulse-generating networks. Proc. Natl. Acad. Sci. USA **101:**6355–6360.
7. **Becskei, A., B. Séraphin, and L. Serrano.** 2001. Positive feedback in eukaryotic gene networks: cell differentiation by graded to binary response conversion. EMBO J. **20:**2528–2535.
8. **Castang, S., S. Reverchon, P. Gouet, and W. Nasser.** 2006. Direct evidence for the modulation of the activity of the *Erwinia chrysanthemi* quorum-sensing regulator ExpR by acylhomoserine lactone pheromone. J. Biol. Chem. **281:**29972–29987.
9. **Chen, M., and R. Weiss.** 2005. Artificial cell-cell communication in yeast *Saccharomyces cerevisiae* using signaling elements from *Arabidopsis thaliana*. Nat. Biotechnol. **23:**1551–1555.
10. **Chmiel, J. F., and P. B. Davis.** 2003. State of the art: why do the lungs of patients with cystic fibrosis become infected and why can't they clear the infection? Respir. Res. **4:**8.
11. **Dhooge, A., W. Govaerts, and Y. A. Kuznetsov.** 2003. MATCONT: a MATLAB package for numerical bifurcation analysis of ODEs. ACM Transact. Math. Software **29:**141–164.
12. **Dockery, J. D., and J. P. Keener.** 2001. A mathematical model for quorum sensing in *Pseudomonas aeruginosa*. Bull. Math. Biol. **63:**95–116.
13. **Dong, Y., L. Wang, J. Xu, H. Zhang, X. Zhang, and L. Zhang.** 2001. Quenching quorum-sensing-dependent bacterial infection by an N-acyl homoserine lactonase. Nature **411:**813–817.
14. **Dong, Y.-H., J.-L. Xu, X.-Z. Li, and L.-H. Zhang.** 2000. AiiA, an enzyme that inactivates the acylhomoserine lactone quorum-sensing signal and attenuates the virulence of *Erwinia carotovora*. Proc. Natl. Acad. Sci. USA **97:**3526–3531.
15. **Egland, K. A., and E. P. Greenberg.** 2001. Quorum sensing in *Vibrio fischeri*: analysis of the LuxR DNA binding region by alanine-scanning mutagenesis. J. Bacteriol. **183:**382–386.

16. **Fagerlind, M. G., S. A. Rice, P. Nilsson, M. Harlén, S. James, T. Charlton, and S. Kjelleberg.** 2003. The role of regulators in the expression of quorum-sensing signals in *Pseudomonas aeruginosa*. J. Mol. Microbiol. Biotechnol. **6:**88–100.
17. **François, P., and V. Hakim.** 2004. Design of genetic networks with specified functions by evolution *in silico*. Proc. Natl. Acad. Sci. USA **101:**580–585.
18. **Fuqua, C., M. R. Parsek, and E. P. Greenberg.** 2001. Regulation of gene expression by cell-to-cell communication: acyl-homoserine lactone quorum sensing. Annu. Rev. Genet. **35:**439–468.
19. **Fuqua, C., S. C. Winans, and E. P. Greenberg.** 1996. Census and consensus in bacterial ecosystems: the LuxR-LuxI family of quorum-sensing transcriptional regulators. Annu. Rev. Microbiol. **50:**727–751.
20. **Fuqua, W. C., and S. C. Winans.** 1994. A LuxR-LuxI type regulatory system activates *Agrobacterium* Ti plasmid conjugal transfer in the presence of a plant tumor metabolite. J. Bacteriol. **176:**2796–2806.
21. **Gardner, T. S., C. R. Cantor, and J. J. Collins.** 2000. Construction of a genetic toggle switch in *Escherichia coli*. Nature **403:**339–342.
22. **Goryachev, A. B., D. Jun Toh, K. B. Wee, T. Lee, H. Bao Zhang, and L. Hui Zhang.** 2005. Transition to quorum sensing in an *Agrobacterium* population: a stochastic model. PLoS Comput. Biol. **1:**0265–0275.
23. **Guet, C. C., M. B. Elowitz, W. Hsing, and S. Leibler.** 2002. Combinatorial synthesis of genetic networks. Science **296:**1466–1470.
24. **Haseltine, E. L., and F. H. Arnold.** 2007. Synthetic gene circuits: design with directed evolution. Annu. Rev. Biophys. Biomol. Struct. **36:**1–19.
25. **Horton, R. M., S. N. Ho, J. K. Pullen, H. D. Hunt, Z. Cai, and L. R. Pease.** 1993. Gene splicing by overlap extension. Methods Enzymol. **217:**270–279.
26. **Isaacs, F. J., J. Hasty, C. R. Cantor, and J. J. Collins.** 2003. Prediction and measurement of an autoregulatory genetic module. Proc. Natl. Acad. Sci. USA **100:**7714–7719.
27. **James, S., P. Nilsson, G. James, S. Kjelleberg, and T. Fagerstrom.** 2000. Luminescence control in the marine bacterium *Vibrio fischeri*: an analysis of the dynamics of *lux* regulation. J. Mol. Biol. **296:**1127–1137.
28. **Kobayashi, H., M. Kaern, M. Araki, K. Chung, T. S. Gardner, C. R. Cantor, and J. J. Collins.** 2004. Programmable cells: interfacing natural and engineered gene networks. Proc. Natl. Acad. Sci. USA **101:**8414–8419.
29. **Kramer, B. P., A. U. Viretta, M. Daoud-El-Baba, D. Aubel, W. Weber, and M. Fussenegger.** 2004. An engineered epigenetic transgene switch in mammalian cells. Nat. Biotechnol. **22:**867–870.
30. **Lazdunski, A. M., I. Ventre, and J. N. Sturgis.** 2004. Regulatory circuits and communication in gram-negative bacteria. Nat. Rev. Microbiol. **2:**581–592.
31. **Lyczak, J. B., C. L. Cannon, and G. B. Pier.** 2002. Lung infections associated with cystic fibrosis. Clin. Microbiol. Rev. **15:**194–222.
32. **Lyon, G. J., and R. P. Novick.** 2004. Peptide signaling in *Staphylococcus aureus* and other gram-positive bacteria. Peptides **25:**1389–1403.
33. **Marié, I., J. E. Durbin, and D. E. Levy.** 1998. Differential viral induction of distinct interferon-alpha genes by positive feedback through interferon regulatory factor-7. EMBO J. **17:**6660–6669.
34. **Mayo, A. E., Y. Setty, S. Shavit, A. Zaslaver, and U. Alon.** 2006. Plasticity of the cis-regulatory input function of a gene. PLoS Biol. **4:**e45.
35. **McKenney, D., K. E. Brown, and D. G. Allison.** 1995. Influence of *Pseudomonas aeruginosa* exoproducts on virulence factor production in *Burkholderia cepacia*: evidence of interspecies communication. J. Bacteriol. **177:**6989–6992.
36. **McMillen, D., N. Kopell, J. Hasty, and J. J. Collins.** 2002. Synchronizing genetic relaxation oscillators by intercell signaling. Proc. Natl. Acad. Sci. USA **99:**679–684.
37. **Miller, M. B., and B. L. Bassler.** 2001. Quorum sensing in bacteria. Annu. Rev. Microbiol. **55:**165–199.
38. **Minogue, T. D., M. Wehland-von Trebra, F. Bernhard, and S. B. von Bodman.** 2002. The autoregulatory role of EsaR, a quorum-sensing regulator in *Pantoea stewartii* ssp. *stewartii*: evidence for a repressor function. Mol. Microbiol. **44:**1625–1635.
39. **Novick, R. P., S. J. Projan, J. Kornblum, H. F. Ross, G. Ji, B. Kreiswirth, F. Vandenesch, S. Moghazeh, and R. P. Novick.** 1995. The agr P2 operon: an autocatalytic sensory transduction system in *Staphylococcus aureus*. Mol. Gen. Genet. **248:**446–458.
40. **Rasmussen, T. B., and M. Givskov.** 2006. Quorum sensing inhibitors: a bargain of effects. Microbiology **152:**895–904.
41. **Reischer, H., I. Schotola, G. Striedner, F. Pötschacher, and K. Bayer.** 2004. Evaluation of the GFP signal and its aptitude for novel on-line monitoring strategies of recombinant fermentation processes. J. Biotechnol. **108:**115–125.
42. **Reverchon, S., M. L. Bouillant, G. Salmond, and W. Nasser.** 1998. Integration of the quorum-sensing system in the regulatory networks controlling virulence factor synthesis in *Erwinia chrysanthemi*. Mol. Microbiol. **29:**1407–1418.
43. **Rosson, R. A., and K. H. Nealson.** 1981. Autoinduction of bacterial bioluminescence in a carbon limited chemostat. Arch. Microbiol. **129:**299–304.
44. **Sayut, D. J., Y. Niu, and L. Sun.** 2006. Construction and engineering of positive feedback loops. ACS Chem. Biol. **1:**692–696.
45. **Schuster, M., M. L. Urbanowski, and E. P. Greenberg.** 2004. Promoter specificity in *Pseudomonas aeruginosa* quorum sensing revealed by DNA binding of purified LasR. Proc. Natl. Acad. Sci. USA **101:**15833–15839.
46. **Shadel, G. S., and T. O. Baldwin.** 1991. The *Vibrio fischeri* LuxR protein is capable of bidirectional stimulation of transcription and both positive and negative regulation of the *luxR* gene. J. Bacteriol. **173:**568–574.
47. **Singh, P. K., A. L. Schaefer, M. R. Parsek, T. O. Moninger, M. J. Welsh, and E. P. Greenberg.** 2000. Quorum-sensing signals indicate that cystic fibrosis lungs are infected with bacterial biofilms. Nature **407:**762–764.
48. **Sitnikov, D. M., G. S. Shadel, and T. O. Baldwin.** 1996. Autoinducer-independent mutants of the LuxR transcriptional activator exhibit differential effects on the two *lux* promoters of *Vibrio fischeri*. Mol. Gen. Genet. **252:**622–625.
49. **Song, H., and L. You.** 2006. Evolving sensitivity. ACS Chem. Biol. **1:**681–682.
50. **Teichmann, S. A., and M. M. Babu.** 2004. Gene regulatory network growth by duplication. Nat. Genet. **36:**492–496.
51. **Trott, A. E., and A. M. Stevens.** 2001. Amino acid residues in LuxR critical for its mechanism of transcriptional activation during quorum sensing in *Vibrio fischeri*. J. Bacteriol. **183:**387–392.
52. **Umulis, D. M., M. Serpe, M. B. O'Connor, and H. G. Othmer.** 2006. Robust, bistable patterning of the dorsal surface of the *Drosophila* embryo. Proc. Natl. Acad. Sci. USA **103:**11613–11618.
53. **Urbanowski, M. L., C. P. Lostroh, and E. P. Greenberg.** 2004. Reversible acyl-homoserine lactone binding to purified *Vibrio fischeri* LuxR protein. J. Bacteriol. **186:**631–637.
54. **Voigt, C. A., D. M. Wolf, and A. P. Arkin.** 2005. The *Bacillus subtilis sin* operon: an evolvable network motif. Genetics **169:**1187–1202.
55. **Wagner, A.** 2005. Circuit topology and the evolution of robustness in two-gene circadian oscillators. Proc. Natl. Acad. Sci. USA **102:**11775–11780.
56. **Wang, Y.-C., and E. L. Ferguson.** 2005. Spatial bistability of Dpp-receptor interactions during *Drosophila* dorsal-ventral patterning. Nature **434:**229–234.
57. **Waters, C. M., and B. L. Bassler.** 2005. Quorum sensing: cell-to-cell communication in bacteria. Annu. Rev. Cell Dev. Biol. **21:**319–346.
58. **Weingart, C. L., C. E. White, S. Liu, Y. Chai, H. Cho, C.-S. Tsai, Y. Wei, N. R. Delay, M. R. Gronquist, A. Eberhard, and S. C. Winans.** 2005. Direct binding of the quorum sensing regulator CepR of *Burkholderia cenocepacia* to two target promoters *in vitro*. Mol. Microbiol. **57:**452–467.
59. **You, L., R. S. Cox III, R. Weiss, and F. H. Arnold.** 2004. Programmed population control by cell-cell communication and regulated killing. Nature **428:**868–871.
60. **Zhou, T., L. Chen, and K. Aihara.** 2005. Molecular communication through stochastic synchronization induced by extracellular fluctuations. Phys. Rev. Lett. **95:**178103. doi:10.1103/PhysRevLett.95.178103.
61. **Zhu, J., M. B. Miller, R. E. Vance, M. Dziejman, B. L. Bassler, and J. J. Mekalanos.** 2002. Quorum-sensing regulators control virulence gene expression in *Vibrio cholerae*. Proc. Natl. Acad. Sci. USA **99:**3129–3134.
62. **Zhu, J., and S. C. Winans.** 1999. Autoinducer binding by the quorum-sensing regulator TraR increases affinity for target promoters in vitro and decreases TraR turnover rates in whole cells. Proc. Natl. Acad. Sci. USA **96:**4832–4837.